UC Irvine
UC Irvine Previously Published Works

Title

Temperature-sensitive magnetic drug carriers for concurrent gemcitabine chemohyperthermia.

Permalink

https://escholarship.org/uc/item/5wd7n0f9

Journal

Advanced healthcare materials, 3(5)

ISSN

2192-2640

Authors

Kim, Dong-Hyun
Guo, Yang
Zhang, Zhuoli
et al.

Publication Date

2014-05-01

DOI

10.1002/adhm.201300209

Peer reviewed

Temperature Sensitive Magnetic Drug Carriers for Concurrent Gemcitabine Chemohyperthermia

Dong-Hyun Kim,
Department of Radiology, Northwestern University, Chicago, IL, USA

Robert H. Lurie Comprehensive Cancer Center, Chicago, IL, USA

Yang Guo,
Department of Radiology, Northwestern University, Chicago, IL, USA

Zhuoli Zhang,
Department of Radiology, Northwestern University, Chicago, IL, USA

Daniel Procissi,
Department of Radiology, Northwestern University, Chicago, IL, USA

Jodi Nicolai,
Department of Radiology, Northwestern University, Chicago, IL, USA

Reed A. Omary, and
Department of Radiology and Radiological Sciences, Vanderbilt University Medical Center, Nashville, TN, USA

Andrew C. Larson
Department of Radiology, Northwestern University, Chicago, IL, USA

Department of Bioengineering, University of Illinois at Chicago, Chicago, IL, USA

Department of Electrical Engineering and Computer Science, Evanston, IL, USA

Robert H. Lurie Comprehensive Cancer Center, Chicago, IL, USA

Department of Biomedical Engineering, Northwestern University, Chicago, IL, USA

International Institute of Nanotechnology (IIN), Northwestern University, Evanston, IL, USA

Dong-Hyun Kim: dhkim@northwestern.edu

Abstract

We sought to improve the efficacy of gemcitabine (GEM) for the treatment of advanced pancreatic cancer via local hyperthermia potentiated via a multi-functional nanoplatform permitting both *in vivo* heating and drug delivery. Herein, we propose a chemohyperthermia approach to synergistically achieve high intra-tumoral drug concentrations while permitting concurrent hyperthermia for more effective tumor cell kill and growth inhibition. Drug delivery and

Correspondence to: Dong-Hyun Kim, dhkim@northwestern.edudhkim0405@gmail.com.

Supporting Information
Supporting Information is available online from the Wiley Online Library or from the author.

hyperthermia were achieved using a hydroxypropyl cellulose (HPC) grafted porous magnetic drug carrier that is MRI visible to permit *in vivo* visualization of the biodistribution. These synthesized magnetic drug carriers produced strong T2 weighted image contrast and permitted efficient heating using low magnetic field intensities. The thermo-mechanical response of HPC permitted triggered GEM release confirmed during *in vitro* drug release studies. During *in vitro* studies, pancreatic cancer cell growth was significantly inhibited (~82% reduction) with chemohyperthermia compared to chemotherapy or hyperthermia alone. Using PANC-1 xenografts in nude mice, the delivery of injected GEM-loaded magnetic carriers (GEM-magnetic carriers) was visualized with both MRI and fluorescent imaging techniques. Chemohyperthermia with intra-tumoral injections of GEM-magnetic carriers (followed by heating) resulted in significant increases in apoptotic cell death compared to tumors treated with GEM-magnetic carriers injections alone. Chemohyperthermia with GEM-magnetic carriers offers the potential to significantly improve the therapeutic efficacy of gemcitabine for the treatment of pancreatic cancer. *In vivo* delivery confirmation with non-invasive imaging techniques could permit patient-specific adjustments therapeutic regimens for improve longitudinal outcomes.

Keywords

chemohyperthermia; drug carrier; gemcitabine; nanoparticles; pancreatic cancer

1. Introduction

Pancreatic cancer is highly aggressive with a median survival of 6 months and 5-year survival rate of only 3%.[1] To date, radical surgical resection remains the only treatment offering an advantage in terms of overall survival benefit (5-year survival ranging from 15 to 25%). However, most patients with pancreatic cancer are not candidates for surgery (only 10–20%).[2] Alternatively, most patients receive gemcitabine (4-amino-1-[(2R,4R,5R)-3,3-difluoro-4-hydroxy-5-(hydroxymethyl)oxolan-2-yl]-1,2-dihydropyrimidin-2-one) chemotherapy, either alone or in concert with various forms of radiotherapy. While gemcitabine chemotherapy has demonstrated the potential to elicit positive clinical responses (23.8% of cases),[3] overall improvements in patient survival rates have been minimal.

Gemcitabine (GEM) has a short plasma half-life (~17 min) and is decomposed into inactive products shortly after infusion due this drug's small molecular weight and hydrophilicity.[4] At a standard dose of 1000 mg/m^2, a patient's plasma GEM concentration drops to roughly 0.4 μg/ml within 1hr after intravenous infusion, well below the 5 μg/ml plasma concentration considered optimal for growth inhibition.[4] Much larger systemic doses may be necessary to achieve therapeutically effective plasma concentrations, but these larger doses would result in a significantly greater risk of toxic side effects.

To overcome intrinsic barriers to efficient drug delivery while reducing the potential for systemic toxicities, an increasing number of studies have recently focused upon the development of targeted drug delivery platforms including phospholipid based liposomes[5], polymeric micelles formed from amphiphilic block copolymers[6], polymer surfactant

polymersomes[7], and covalent-linked structures, such as polymer-drug conjugates[8], dendrimers[9], mesoporous silica[10] and carbon nanotubes[11]. The advantages of these drug carriers include protection of the drug from degradation, increased drug solubility, prolonged drug exposure times, selective drug delivery to targeted tissues (targeting ligands and/or 'enhanced permeability and retention' effects[12]) and the potential to stimulate drug release while also imaging delivery to the intended targets. The ultimate goal of these approaches is achieving superior therapeutic outcomes while decreasing toxicity and limiting drug resistance.

Hyperthermia (typically defined as temperature increases to >43°C but generally < 50°C) can be used as a synergistic therapeutic modality inhibiting active membrane transport of ions, reducing metabolism, pH and inhibiting angiogenesis while slowing down or even blocking DNA replication leading to malignant cell death and tumor destruction.[13] Recent studies have shown that many chemotherapeutic drugs (e.g. doxorubicin and cisplatin) interact synergistically with concurrent hyperthermia resulting in enhanced cytotoxic effects.[14] Hyperthermia combined with GEM chemotherapy (concurrent GEM chemohyperthermia) may offer a promising method for the treatment of pancreatic cancer. When combined with a temperature sensitive drug delivery platform, hyperthermia could be used to both stimulate drug release as well as sensitize tumor tissues to the delivered tumoricidal agent.

The ideal drug delivery platform for GEM chemohyperthermia should permit selective drug delivery and/or enhanced tumor tissue retention, hyperthermia, stimulated drug release (concurrent to increases in temperature), and imaging for quantitative estimates of drug delivery to the targeted tumors. For this purpose, porous silica-coated magnetic cluster nanoparticles were synthesized with temperature-sensitive hydroxypropyl cellulose (HPC) grafted to the surface thus producing a drug delivery platform for GEM chemohyperthermia (Fig. 1). The purpose of our study was to investigate the magnetic heating, GEM release, and magnetic resonance imaging (MRI) properties of this drug delivery platform before subsequently validating the efficacy of concurrent chemohyperthermia in *in vitro* settings prior to *in vivo* studies in a xenograft animal model demonstrating the feasibility of this approach for the treatment of pancreatic cancer.

2. RESULTS

2.1. Magnetic USPIO Cluster Characteristics

7±1 nm USPIO nanoparticles formed 59±6 nm clusters when coupled with the polyacrylic acid (Fig. 1 and Fig. 2a). The USPIO solution was water dispersible and stable in aqueous solution with a surface charge of −48.7 mV (zeta potential). Room temperature superparamagnetic behavior of these USPIO clusters was maintained with a measured saturation magnetization of 61 emu/g (supplementary Fig. S1).

2.2. Temperature Sensitive Magnetic Drug Carrier Characteristics

The USPIO clusters were encapsulated within a porous silica shell and HPC capping material to form temperature sensitive magnetic drug carriers (Fig. 1). TEM images of the Si

coated USPIO clusters demonstrated a discrete core/shell structure with 59±6 nm USPIO cluster cores and a silica shell 18±2 nm in thickness (Fig. 2b). These particles were further etched to provide a porous structure conducive to drug-loading; these ~5 nm pores are shown within TEM image in Fig. 2c. BET surface area of the etched silica shell encapsulated USPIO clusters was 113.5 m^2/g, which was increased from 14.7 m^2/g of non-etched silica shell encapsulated USPIO clusters, with generated porous structures. Residual PVP polymer on the porous silica shell was utilized for further modification with a temperature sensitive hydroxypropyl cellulose (HPC) polymer. Hydrogen bonding between HPC and PVP was confirmed with FTIR spectra (Fig. 2e). Absorption bands within the FTIR spectra show hydroxyl-stretching vibrations, demonstrative of hydrogen bonds between the PVP and HPC. Broad transmission bands were observed between wavelengths of 3600 and 3100 cm^{-1} due to the stretching of hydroxyl groups in the spectrum of HPC. Transition bands between wavelengths of 1000 and 1100 cm^{-1} typical for ether linkages of HPC, were found only in the spectrum of the HPC grafted particles. The magnetic drug carriers including polymers, silica and magnetic clusters demonstrated a saturation magnetization of 20 emu/g. At 300 K, hysteresis behavior disappeared; these drug carriers exhibited superparamagnetic behavior with no coercivity or remanence (Fig. 3a). A superparamagnetic blocking temperature (T_B) of 30 K was determined between the zero-field cooled/field cooled (ZFC/FC) curves (Fig. 3a (**inset**)). The temperature of the sample solution upon magnetic heating (13.9 kA/m (175 Oe), 199 kHz) was monitored; temperature was found to rapidly increase surpassing the therapeutic threshold required for hyperthermia (~45°C) within 100 sec (Fig. 3b). The calculated specific absorption rate (SAR)[15] for these magnetic drug carriers was 183 w/g. Next, we measured the temperature sensitive size changes of these magnetic drug carriers over a range from 25 to 47°C (physiologically relevant temperature range for anticipated hyperthermia therapeutic applications). For magnetic drug carrier concentrations of 1 mg/ml and pH 7, significant size changes were evident (Fig. 4a). The size of the magnetic drug carriers decreased at roughly 41 °C (LCST) and then with a further increase in temperature, particle size increased. However, with prolonged exposure time (~5 mins) above 41°C the average hydrodynamic size increased significantly. Temperature sensitive size changes were not observed for magnetic drug carriers lacking HPC grafting; the latter particles demonstrated stable hydrodynamic sizes during increases in temperature.

2.3. *In Vitro* Temperature Responsive Drug Release

GEM drug loading efficiency for these HPC grafted magnetic drug carriers was ~66% with initial GEM loading of 20 wt%. *In vitro* release was evaluated at two different temperatures (37 and 45 °C) as shown in Fig. 4b. At both temperatures, a two-phase release pattern was observed with an initial fast 'burst' release followed by a relatively slower, sustained release period. Drug release was more rapid at 45 °C with cumulative drug release of ~37% after 180 mins; only 8 % of the drug was released over a period of 180 mins at 37 °C (Fig. 4b). By comparison, bare magnetic drug carriers released the similar quantities of GEM at the either temperatures (Fig. 4b). Pronounced temperature sensitive drug release was also observed during periods of dynamic temperature cycling between 37 and 43°C (Fig. 4c). After 4hours spontaneous drug release, we applied a heating cycle to increase solution temperature to 45°C. The drug release rate rapidly increased during the heating cycle with

~3% released during this 45 min interval. When solution cooled to 37°C again, drug was released only ~0.3% during this 30 min.

2.4. *In vitro* uptake and cytotoxicity of GEM loaded magnetic drug carriers

Rhodamine isothiocyanate (RITC) labeled magnetic drug carriers were readily visible with confocal laser scanning microscopy. After a 4-hour incubation period, cellular uptake of the magnetic drug carriers was confirmed; minimal magnetic drug carrier uptake was observed after shorter 1hr incubation period (Fig. 5a). Cellular uptake of the drug carrier was also confirmed with cross-sectional Z-stack confocal microscopy images (Supplementary Fig. S2). The cytotoxicity of these magnetic drug carriers was measured in PANC-1 cells by MTT assay prior to subsequent chemohyperthermia tests. The unloaded magnetic drug carriers and magnetic clusters were non-toxic with 80 % cell viability maintained at concentrations of up to 2 mg/ml (Supplementary Fig. S3).

2.5. Concurrent GEM Chemohyperthermia for In vitro PANC-1 Cell Growth Inhibition

PANC-1 cell growth inhibition due to chemotherapy, hyperthermia, and chemohyperthermia upon exposure to the magnetic drug carriers was evaluated with MTT assays. GEM-magnetic drug carriers (1 mg/ml (loaded GEM: ~60 ug)) without hyperthermia heating inhibited the growth of PANC-1 cells by spontaneous initial drug release during 1–6 hour treatment periods (Fig. 5b). Cell viability was 80 % after 1 hour exposure but significantly reduced to less than 65% after 5 and 6 hour exposure periods ($p<0.05$). These limited cell growth inhibition effects were significantly enhanced with the application of concurrent hyperthermia. PANC-1 cells were exposed to GEM-magnetic drug carriers for 3 hours and then further treated with hyperthermia (heating to 43 or 45 °C) for another 30 mins (Fig. 5b inset depicts representative controlled heating cycle). When magnetic heating to 42 and 45 °C was applied after a 3-hour exposure to the GEM-magnetic drug carriers, cell viability significantly decreased to 21 % and 12 %, respectively (>30% decrease in PANC-1 cell viability compared to either chemotherapy or hyperthermia alone).

2.6. Phantom and *In vivo* Multimodal MRI and Fluorescence Imaging

The measured r_2 relaxivity of the synthesized magnetic drug carriers (302 mM^{-1}s^{-1}) was 3 times higher than the r_2 relaxivity measured for non-clustered 7 nm USPIO (116 mM^{-1}s^{-1}) (Fig. 6a). To verify the *in vivo* effectiveness of the magnetic drug carriers as T_2 contrast agents, T_2-weighted images of mice (n=3) were acquired before/after intravenous injection of the magnetic drug carriers (5 mg/ml;100 ul) (Fig. 6b). We investigated the potential for *in vivo* imaging of the magnetic drug carriers after systemic administration and passive tumor accumulation or following direct intra-tumoral injection. Within T2-weighted images, intra-tumoral signal reductions were observed 2 hrs following intravenous injection of the magnetic drug carriers (Fig. 6b). In color-coded T2 map, intra-tumoral deposition of the magnetic carriers is depicted as a dark blue region (Fig. 6b). The fluorescence of the IV injected NIR fluorescent dye labeled magnetic drug carriers represented the appreciable accumulation of the sample in tumors through the EPR effect. The accumulation in the rest of the organs, including liver and kidney, showed the typical accumulation in NIR fluorescence imaging (Fig. 6c).

2.7. *In vivo* Concurrent GEM Chemohyperthermia in PANC-1 Mouse Model

4 groups (5 mice in each group), Group 1 (chemohyperthermia), Group 2 (hyperthermia), Group 3 (chemotherapy) and Group 4 (Control group), were used to evaluate the anti-cancer effects of chemohyperthermia. GEM-magnetic drug carriers (5 mg/ml; 100 ul) (Groups 1 and 3) or only magnetic drug carriers (Group 2) were delivered directly into the tumor. No evidence of injection site reactions such as superficial redness, drug allergy, infection, ulceration, erosion, or necrosis of skin were observed in all groups. *In vivo* MRI and NIR fluorescent imaging confirmed successful magnetic drug carrier delivery to the tumor region in groups 1, 2 and 3 (representative images in Fig. 7a and 7b). H&E staining demonstrated that most cell membrane structures remained relatively well preserved for tumor tissues in Groups 2, 3 and 4 mice whereas marked inflammation and necrosis was observed for tumor tissues in Group 1 mice (Fig. 7c). Less intense staining and/or swelling were observed for many tumor cells from chemohyperthermia group suggestive of significant damage to these tissues. Apoptosis was also observed, shrunken cells with condensed cytoplasm (Group 1, TUNEL staining in Fig. 7c). Remarkably, xenografts treated with chemohyperthermia (Group 1) revealed much higher apoptotic levels than the Group 2, 3 and 4 ($p < 0.05$). Cells in the control Group 4 tumors showed the lowest degree (7.2 %) of apoptosis. Group 2 (hyperthermia) and Group 3 (chemotherapy) showed only 14.7% and 17.5% apoptotic cells, respectively. In contrast, Group 1 (chemohyperthermia) demonstrated significantly increased levels of apoptosis (38.0%; $P < 0.05$) (Fig. 7d).

3. Discussion

Few effective therapeutic approaches are available for treating advanced inoperable pancreatic cancer. Chemotherapy with GEM can elicit positive responses but overall improvements in patient survival rates have been minimal. Both nanoparticle drug-delivery platforms and hyperthermia approaches offer the potential to improve the efficacy of GEM chemotherapy. For this purpose, porous magnetic drug carriers were synthesized with temperature-sensitive HPC grafted to the surface. The magnetic heating, drug release, and imaging properties of this drug delivery platform were investigated to establish the feasibility of using these nanoparticles for GEM chemohyperthermia. Subsequent *in vitro* studies validated that concurrent hyperthermia with these temperature-sensitive magnetic drug carriers can significantly enhance GEM cytotoxicity and *in vivo* studies validated the potential to visualize targeted delivery to tumors and the feasibility of eliciting superior therapeutic responses of the targeted concurrent GEM chemohyperthermia.

The synthesized USPIO clusters as a core in the magnetic drug carriers demonstrated a much stronger response to external magnetic fields than the response demonstrated by non-clustered USPIO nanoparticles due to a much higher magnetization per particle. Accordingly, the r_2 relaxivity of the synthesized USPIO clusters was 3 times greater than the r_2 relaxivity observed for non-clustered 7 nm USPIO particles. These results are concordant with prior studies evaluating the MR contrast effects of magnetic clusters.[16] The heating efficiency of these magnetic clusters was also significantly higher compared to the non-clustered USPIO particles. The high performance of the USPIO clusters suggests the

suitability of these materials to serve as an efficient functional component of a drug-carrier platform.

The USPIO clusters were further modified with a porous silica shell and HPC as a capping material. Prior studies have demonstrated that silica is a promising platform for the delivery of anti-cancer agents.[17] Porous silica materials offer a large internal volume for drug loading, robust and defined structure for the containment of the drug molecules, and the ability to release the drugs under specific conditions (altered pH or temperature)[18]. In our study, PVP polymer on the surface of the porous silica shell was well utilized for grafting with a temperature sensitive HPC polymer. HPC as a water-soluble, biodegradable, natural cellulose with excellent biocompatibility has been included in a number of medical devices already approved by the FDA.[19] Because the HPC contains a large number of proton-donating hydroxyl groups within its structure, hydrogen bonding is readily achieved between proton accepting carbonyl groups in PVP on the porous silica shell and the partially oxidized HPC.[20] We also measured the zeta-potential of the samples to verify grafting HPC polymers. The surface of magnetic drug carriers was weak negatively charged (zeta-potential =−2.8 mV) with coated PVP but the grafted HPC containing a large number of hydroxyl groups was confirmed with an increased negative charge (−32.5 mV at pH ~7).

It is known that HPC exhibits a lower critical solution temperature (LCST) in water, so HPC shrinks when heated up to its LCST, which is ≈41°C.[21] We confirmed this temperature sensitive property by measuring temperature sensitive size changes of the magnetic drug carriers over a range from 25 to 47 °C. It was found that the particle size of the magnetic carriers was steeply decreased around 41 °C (LCST), then particle size was increased again by increasing temperature further. Prolonged exposure time (5 min) above 41 °C increased the average hydrodynamic size significantly, which is indicative of nanoparticle aggregation.[22] Increasing hydrophobicity of the HPC on the surface of the magnetic drug carriers is believed to drive such aggregation. This temperature sensitive hydrodynamic size change was reversible with temperature cycling, specifically, drug carrier size was able to be decreased with the application of a cooling cycle (dropping temperature from 50 to 25 °C) while shaking samples and allowing for a 1 min equilibration time and the thermo-mechanical behavior was directly utilized for the controlled drug release. As we expected, a much faster release of GEM was observed at 45 °C in comparison drug release at 45 °C and 37 °C. Collapse of the HPC polymer caused by temperature triggered water molecule dissociation increased the diffusion of GEM incorporated in the porous structure thus accelerating the rate of drug release. It offers to perform concurrent GEM chemohyperthermia therapy that can release more anti-cancer GEM drug upon magnetic hyperthermia therapeutic heating.

The therapeutic advantage of GEM chemohyperthermia therapy with the synthesized GEM loaded magnetic carriers was confirmed with *in vitro* cell studies. When magnetic heating to 42 and 45 °C were applied for 30 mins, cell viabilities were dramatically decreased from 76% to 21 % and 12 %, respectively. More importantly, the GEM chemohyperthermia induced 3~5 times more Panc-1 cell toxicity than chemotherapy or hyperthermia alone. In the presence of the oscillating field, the local heating in the magnetic drug carriers facilitated

the release of GEM from the silica pores, inducing higher cell growth inhibitory effects than chemotherapy or hyperthermia (Fig. 5b).

Prior to *in vivo* GEM chemohyperthermia experiments, the potential for *in vivo* imaging of the magnetic carriers was investigated. It may be imperative to directly assess the distribution of these drug carriers as well as the magnitude of their accumulation at tumor sites as this information could be valuable for optimization of individual patient's treatment protocols.[23] The relaxivity of these magnetic carriers that was ~3 fold higher than commercially available superparamagnetic iron oxide nanoparticles (5 nm r-Fe_2O_3 core; 104 $mM^{-1}S^{-1}$) (Feridex, Bayer HealthCare Pharmaceuticals)[24] and 7 nm USPIO nanoparticles (116 $mM^{-1}s^{-1}$). These drug carriers induced significant signal reductions within T_2 weighted images indicative of deposition at multiple sites within and adjacent to the tumor(s) (Fig. 6b and Fig. 7a). Accumulation of the magnetic drug carriers in the tumor tissues was also confirmed using NIR dye loaded magnetic carriers.

Finally, to demonstrate *in vivo* anti-cancer effects of GEM-chemohyperthermia, GEM-magnetic carriers were injected directly into the tumor center prior to application of an alternating magnetic field (199 kHz-175 Oe in bio-safe range not inducing non-specific heating).[25] We found that concurrent chemohyperthermia significantly increased tumor cell death in tumor tissues. We performed TUNEL staining to measure proportions of DNA fragmented apoptotic cancer cells in the tumor tissues from mice undergoing the four different prescribed treatment protocols. Due to massive tumor volumes compared with small volume (100 ul) of GEM magnetic microspheres and relatively short-term observance, the level of apoptosis area was low (38%) with GEM-chemohyperthermia treatment. However, compared to chemotherapy or hyperthermia alone, GEM-chemohyperthermia was clearly more effective for eliciting tumor cell apoptosis. Although investigation of the specific synergistic mechanisms for these improved outcomes was beyond the scope of this initial *in vivo* feasibility study, induced Hsp70/Hsp32 proteins and over-acidation during hyperthermia may cause pancreatic cancer cells to be more sensitive to GEM chemotherapy. [26]

4. Conclusion

Biocompatible temperature-sensitive magnetic drug carriers for heating, controlled drug delivery, and imaging were successfully synthesized and characterized. Both *in vitro* studies and *in vivo* pancreatic cancer xenograft studies demonstrated the potential to use concurrent chemohyperthermia with GEM-magnetic carriers to induce superior anti-cancer effects to hyperthermia and chemotherapy alone. In addition to permitting local heating upon exposure to AMF, these drug carriers permitted *in vivo* MRI for confirmation of tumor delivery. These initial encouraging results strongly suggest that chemohyperthermia with GEM-magnetic carriers may offer an important, innovative new approach for more effective treatment of pancreatic cancer.

5. Experimental Section

Materials

Ferric chloride (FeCl$_3$), 25% ammonium hydroxide solution, diethylene glycol (DEG), sodium hydroxide, poly acrylic acid (PAA), polyvinyl pyrollidone (PVP), hydroxypropyl cellulose (HPC, average Mw ~ 80k), tetraethylorthosilicate (TEOS), sodium periodate (NaIO$_4$), ammonium hydroxide (NH$_4$OH;28–30wt%) and rhodamine isothiocyanate (RITC) were purchased from Sigma-Aldrich. Gemcitabine (GEM) was purchased as lyophilized powder in vials containing 500 mg of GEM as chloride salt from LC laboratories (MA, USA). For MTT assay, 3-[4,5-dimethylthiazol-2-yl]-3,5-diphenyltetrazolium bromide salt and dimethylsulfoxide (DMSO) were purchased from Sigma Chemicals Co. (St. Louis, USA). Cyto780 fluorescent dye for animal imaging was purchased from Cytodiagnostics (Ontario, Canada).

Synthesis of Temperature Sensitive MRI-Visible Magnetic Drug Carriers

Ultrasmall superparamagnetic iron oxide (USPIO) clusters were synthesized using a high temperature hydrolysis reaction[27], and then coated with a layer of silica through a modified Stöber process.[28, 29] Briefly, a NaOH/DEG stock solution was prepared by dissolving 2 g of NaOH in DEG (20 ml). The solution was heated to 120 °C for 30 mins under nitrogen, cooled, and kept at 70 °C. A mixture of FeCl$_3$ (0.4 mmol), PAA (4 mmol), and DEG (17 ml) was heated to 220 °C in a nitrogen atmosphere for 30 min with vigorous stirring to form a transparent solution. NaOH/DEG stock solution (2 ml) was injected into the hot mixture. The resulting mixture was further heated for 1 h to yield ~60 nm USPIO clusters composed of ~7 nm USPIO. The final products were washed with a mixture of deionized water and ethanol 3 times and re-dispersed in deionized water. Silica coated USPIO clusters were then prepared via the method described by Qiao et al.[28] A 3mL solution of the USPIO clusters was mixed with 20 mL ethanol and 1 mL NH$_4$OH under vigorous magnetic stirring. TEOS (0.1 mL) was injected into the solution every 20 min until the total amount of TEOS reached 0.3 mL. After washing with ethanol three times, the products were redispersed in 20 mL deionized water. To increase the porosity of the silica shell, the silica coated USPIO clusters were mixed with 1g PVP, and then refluxed for 3h. Upon cooling the mixture down to room temperature, NaOH aqueous solution (5 mL, 0.20 g/mL) was injected to the system to initiate etching. After etching for 20 mins, the particles were collected by centrifugation and washed 3 times with DI water. Then, HPC was grafted on the porous silica shell via hydrogen bonding with the remained PVP molecules. 2 g of NaIO$_4$ was dissolved in 10 ml water using ultrasonication and filtered to remove the excess NaIO$_4$ after 1 hour. To partially oxidize HPC polymer chains, 10 wt% solution of HPC was added to the saturated NaIO$_4$ solution and mixed for 18 hr in the dark at room temperature. To graft HPC onto the PVP coated silica surface, 10 ml of the PVP-porous silica USPIO clusters solution (10 mg/ml) was added to partially oxidized HPC solution (0.2 wt%). The solution was mixed for 12 hr then washed 3 times with water using centrifugation cycles at 8,500 rpm. Finally, these synthesized magnetic drug carriers were collected and redispersed in water.

Magnetic Drug Carrier Characterization

The crystal structure, size and magnetic properties of the synthesized samples were characterized using an X-ray diffractometer (XRD; Scintag XDS-2000), vibrating sample magnetometer (VSM; Model 7400, Lake Shore, Westerville, OH, USA) and transmission electronic microscope (TEM; FEI Tecnai Spirit G2) operating at 120 kV. BET (Brauauer, Emmett and Teller) gas adsorption was measured to determine the surface area of the particles using a Micromeritics Tristar 3000 volumetric adsorption analyzer. The IR spectra of the samples were recorded with a PerkinElmer Instruments Spectrum Spotlight 300. The temperature dependent mean particle size and size-distribution of the samples were investigated with dynamic light scattering (DLS) using a Zetasizer Nano-S (Malvern, Herrenberg, Germany) equipped with a 4 mW HeNe laser.

GEM Loading and Release Studies

GEM (~2 mg) and the synthesized magnetic drug carriers (10 mg) were mixed in 10 mL of distilled water, which was stirred vigorously at 45° C for 3 hours and overnight at room temperature. The solution was evaporated in vacuum. The resulting dried mixture was washed 3 times with water against an excess amount of distilled water to remove unloaded drugs and lyophilized. The aqueous sample solution (1 mg/ml;1 ml) was placed into a membrane bag (Spectra/Por MWCO 8,000, Spectrum, Los Angeles, CA, USA) and then immersed in 40 ml of PBS (Phosphate Buffer Solution, pH 7.2). The temperature of the medium was maintained at 37 °C or 43 °C using a water bath. At specific time intervals, PBS medium (1 ml) was extracted and replaced with fresh medium. The concentration of released GEM was determined using a UV-Vis spectrometer (Lambda 950, Perkin Elmer, Waltham, MA, USA) at 275 nm. Heating of the magnetic drug carriers (1 mg/ml, 1ml) and GEM release was investigated via the application of an AC magnetic field at 199 kHz (175 Oe) for 1h. For this purpose, a 2.3 kW power supply (Ameritherm EASYHEAT 0224, Scottsville, NY, USA) was used with a remote heating station and custom-made coil (4 turns, diameter 8 cm, height 9 cm). The solution temperature in a glass vial was monitored with a fluoro-optic fiber thermometer (Photon Control, BC, Canada); temperature was recorded every 10 s after switching on the power supply. Temperature dependent GEM release was measured using the UV-Vis spectrophotometer.

MRI Relaxivity Measurements

Imaging phantoms were prepared by diluting samples of the magnetic drug carriers in 0.1% agarose at particle concentrations that ranged from 0.02 to 0.45 mMFe. The atomic Fe concentrations of the stock solutions were determined using inductively coupled plasma mass spectroscopy (ICP-MS, Perkin Elmer, Waltham, MA, USA). MRI experiments were performed using a 7 Tesla MRI scanner (Clinscan, Bruker, Billerica, MA, USA). Images were acquired using a phased-array coil and a T_2-weighted multi-echo fast spin-echo sequence (TR=5000 ms). This sequence was used to rapidly collect a series of images at different echo-times (32 echo-times ranging from 15ms to 480ms). The T_2 relaxation time for each phantom vial was calculated by fitting the signal decay curve to the nonlinear mono-exponential function $S(TE)=M_0exp(-TE/T_2)$ with TE = echo-time and S(TE) the mean signal measured within the phantom vial at a given TE.

Cell Lines and Cell Culture

The human pancreatic carcinoma cell line PANC-1 (ATCC, CRL 1687) was obtained from American Type Culture Collection (ATCC, Manassas, VA, USA). Cells were cultivated in 75 cm^2 culture flasks and maintained in RPMI 1640 culture medium supplemented with fetal bovine serum (FBS), 100 U/ml penicillin and 100 U/ml streptomycin, at 37 °C in a humidified atmosphere containing 5% CO_2.

Biocompatibility of GEM Loaded Magnetic Drug Carriers

For cytotoxicity studies, 7.5×10^3 cells (100 μL) were transferred into each well and incubated to allow 70% confluence 48h after initial plating. Cells were washed with PBS and then exposed to either unloaded or GEM-magnetic drug carriers in serum-free culture medium (200 μL) achieving final drug carrier doses of 0.01 ~ 2 mg/ml per well. Cells were then incubated in this medium at 37 °C for 24 h. Dose-dependent drug carrier impacts upon cell viability was determined with MTT assay. For MTT assay, the treated cells were washed three times with PBS and incubated with MTT media solution (0.5 mg/mL) for 4 h at 37 °C. The formazan dye crystals generated by the live cells were dissolved in DMSO, and the absorbance values at 570 nm determined using a microplate reader (SpectraMax M5 Multi-Mode Microplate Reader) with absorbance at 655 nm serving as a reference. Cell viability was calculated by comparing the absorbance of drug carrier treated wells to that of the control wells.

Fluorescence Imaging of In vitro Cellular Uptake

RITC labeled magnetic drug carriers (5 mg/ml) were prepared.[30] To study gross cellular interactions of the magnetic drug carriers, 3×10^4 PANC-1 cells were seeded onto L-lysine treated glass cover slides and incubated for 24h at 37°C in 5% CO_2 prior to addition of the magnetic drug carriers. Separate samples of the PANC-1 cells were exposure to these particles for 3 and 24 h. Next, the exposure medium was removed and all samples washed 3 times with PBS and fixed for 20 min in 4% neutral buffered formalin solution. Cell nuclei were stained with 4',6-diamidino-2-phenylindole (DAPI blue). A confocal laser-scanning microscope (Carl Zeiss LSM 510 UVMETA, Thornwood. NY) was then used to capture images of the intracellular environment and the sub-cellular localization of the fluorescently labeled magnetic drug carriers. For multi-color fluorescent microscopy, samples were excited with 364 nm (blue channel), 488 nm (green channel), and 543 nm (red channel) lasers.

Concurrent GEM Chemohyperthermia for In vitro PANC-1 Cell Growth Inhibition

The cell growth inhibitory effects of chemotherapy, hyperthermia, and chemohyperthermia using the magnetic drug carriers were evaluated using an MTT assay. Both unloaded and GEM-magnetic drug carriers were used for these studies. First, to investigate chemotherapeutic effects at 37°C, separate samples of the PANC-1 cells (7.5×10^3 cells in 200 μL of culture media) were incubated with either loaded or unloaded magnetic drug carriers at concentrations of 1 mg/ml for 1, 3, 5 or 6 hours. For concurrent chemohyperthermia, additional cell samples were exposed to the GEM-magnetic drug carriers for 3 hours and then further treated with hyperthermia (magnetic field induced

heating to 43 or 45 °C for 30 mins, stable temperatures maintained via real-time adjustment to applied field). After heating, cells were washed three times with PBS (100 μL), and fresh growth medium added to the plates. Cells were then further incubated in the medium at 37°C, and the impacts upon cell viability were evaluated with an MTT assay.

PANC-1 Xenograft Animal Model

BALB/c nude mice (6–8 weeks old) were purchased from Charles River laboratories (Wilmington, MA). All animals were housed under pathogen-free conditions in laminar flow isolation units under alternate dark and light cycles. Animals were maintained on food and water ad libitum. Animal procedures were performed in accordance with guidelines of the National Institutes of Health and were approved by the Northwestern University Animal Use and Care Committee. Tumor-bearing mice were prepared by injecting a suspension of 1×10^7 PANC-1 cells in physiological saline (100 μL) into the subcutaneous dorsa. The tumor size was measured non-invasively using calipers.

In vivo Multimodal MRI and Fluorescence Imaging

When the tumor sizes increased to 8–10 mm after approximately 4 weeks, magnetic drug carriers were administered (100uL, 5mg/mL) either intravenously via tail vein injection (n=3) or intra-tumorally with percutaneous injection (n=3). Two additional mice (n=2) received sterile saline injections to serve as controls. Imaging was performed using a 7T MRI scanner (Clinscan, Bruker, Billerica, MA, USA) and an IVIS® Spectrum system from Caliper (Hopkinton, MA). Each mouse underwent baseline MRI scans prior to injection of the magnetic drug carriers and MR imaging was then repeated 1h post-injection. Intra-tumoral accumulation of the drug carriers was confirmed within fluorescent images acquired using the IVIS® system. For fluorescent imaging property, amine terminated cyto780 fluorescent dye (60 uM) was labeled on the magnetic drug carriers (0.8 mg) using EDC/NHS chemistry (Thermoscientific, USA). Fluorescence imaging with excitation/emission (783nm/800nm) was performed both in vivo and ex vivo after harvesting tumor, peri-tumoral muscle, liver, spleen, and kidney tissues (4hrs after initial drug carrier injection). These tissue specimens were placed on non-fluorescent black Strathmore Artagain paper (Neenah, WI) for fluorescence imaging performed using a raster scanning step size of 1mm. Region of interest (ROI) were drawn to record the mean fluorescent emission at 800nm using Living Image® software (ver. 4.0).

In vivo Concurrent GEM Chemohyperthermia in PANC-1 Mouse Model

Pancreatic xenograft tumors (8–10mm) were grown in a second set of mice for GEM-chemohyperthermia procedures. 20 mice were randomly divided into 4 groups (n=5 mice for each group). Group 1 (chemohyperthermia) received a 100 uL intra-tumoral injection of GEM-magnetic carriers (5 mg/ml) prior to magnetic heating. Group 2 (hyperthermia) received a 100 uL intra-tumoral injection of unloaded magnetic drug carriers (5 mg/ml) prior to magnetic heating. Group 3 (chemotherapy) received a 100 ul intra-tumoral injection of GEM-magnetic carriers (5 mg/ml) but were not subjected to magnetic heating procedures. Group 4 (Control group) received a 100 ul intra-tumoral injection of saline. Imaging was performed using a 7T MRI scanner (Clinscan, Bruker, Billerica, MA, USA) and an IVIS® Spectrum system from Caliper (Hopkinton, MA). Each mouse underwent baseline MRI

scans and fluorescent imaging prior to injection of the magnetic drug carriers and MR imaging was then repeated 1h post-injection. Two hours after injection, mice in Groups 1 and 2 underwent magnetic heating procedures (199 kHz, 175 Oe field applied for 30 mins). Mice were euthanized 4 hours after drug-carrier or sham saline injection. At necropsy, tumor tissues were collected, fixed in formalin, embedded, sectioned (5 μm slices), and stained with hematoxylin and eosin (H&E), Prussian blue and Terminal deoxynucleotidyl transferase dUTP nick end labeling (TUNEL) staining for assessment of cell proliferation and apoptosis. Slides were examined using a Zeiss Axioskop upright fluorescence microscope. For quantification of TUNEL expression, the number of positive cells was counted in 5 random regions and divided by the total number of cells for each tumor slice. All slides were also qualitatively assessed according to established cytomorphological criteria for apoptosis. Both the total number of cells and the number of apoptotic (TUNEL stained) cells in each examined tumor specimen were counted to calculate percentages (ratio between number of apoptotic cells and total number of cells counted).

Statistical Analysis

All results are expressed as mean±standard deviation. Comparisons between groups were performed using one-way analysis of variance (ANOVA). A value of $p < 0.05$ was considered statistically significant.

Supplementary Material

Refer to Web version on PubMed Central for supplementary material.

Acknowledgments

References

1. Jemal A, Siegel R, Xu JQ, Ward E. N. C. Institute, 2010. Ca-Cancer J Clin. 2010; 60:277. [PubMed: 20610543] Kleeff J, Michalski C, Friess H, Buchler MW. Pancreas. 2006; 33:111. [PubMed: 16868475]

2. Johnson JI, Decker S, Zaharevitz D, Rubinstein LV, Venditti J, Schepartz S, Kalyandrug S, Christian M, Arbuck S, Hollingshead M, Sausville EA. Brit J Cancer. 2001; 84:1424. [PubMed: 11355958]

3. Burris HA, Moore MJ, Andersen J, Green MR, Rothenberg ML, Madiano MR, Cripps MC, Portenoy RK, Storniolo AM, Tarassoff P, Nelson R, Dorr FA, Stephens CD, VanHoff DD. J Clin Oncol. 1997; 15:2403. [PubMed: 9196156]

4. Eli Lilly and Co, Eli Lilly and Co. 1997

5. Allen TM. Drugs. 1998; 56:747. [PubMed: 9829150] Drummond DC, Meyer O, Hong KL, Kirpotin DB, Papahadjopoulos D. Pharmacol Rev. 1999; 51:691. [PubMed: 10581328]

6. Kabanov AV, Batrakova EV, Alakhov VY. J Control Release. 2002; 82:189. [PubMed: 12175737] Rangel-Yagui CO, Pessoa A, Tavares LC. J Pharm Pharm Sci. 2005; 8:147. [PubMed: 16124926]

Torchilin VP. Cell Mol Life Sci. 2004; 61:2549. [PubMed: 15526161] Wang J, Mongayt D, Torchilin VP. J Drug Target. 2005; 13:73. [PubMed: 15848957]

7. Discher BM, Won YY, Ege DS, Lee JCM, Bates FS, Discher DE, Hammer DA. Science. 1999; 284:1143. [PubMed: 10325219]

8. Dharap SS, Qiu B, Williams GC, Sinko P, Stein S, Minko T. J Control Release. 2003; 91:61. [PubMed: 12932638] Duncan R, Gac-Breton S, Keane R, Musila R, Sat YN, Satchi R, Searle F. J Control Release. 2001; 74:135. [PubMed: 11489490] Kopecek J, Kopeckova P, Minko T, Lu ZR, Peterson CM. J Control Release. 2001; 74:147. [PubMed: 11489491] Vasey PA, Kaye SB, Morrison R, Twelves C, Wilson P, Duncan R, Thomson AH, Murray LS, Hilditch TE, Murray T, Burtles S, Fraier D, Frigerio E, Cassidy J. C. R. C. P. I. I. Comm. Clin Cancer Res. 1999; 5:83. [PubMed: 9918206]

9. Choi Y, Baker JR. Cell Cycle. 2005; 4:669. [PubMed: 15846063] Patri AK, Kukowska-Latallo JF, Baker JR. Adv Drug Deliver Rev. 2005; 57:2203.

10. Lee JE, Lee N, Kim T, Kim J, Hyeon T. Accounts Chem Res. 2011; 44:893.Mal NK, Fujiwara M, Tanaka Y. Nature. 2003; 421:350. [PubMed: 12540896] Yang P, Gai S, Lin J. Chem Soc Rev. 2012; 41:3679. [PubMed: 22441299] Kang X, Cheng Z, Yang D, Ma P, Shang M, Peng C, Dai Y, Lin J. Adv Funct Mater. 2012; 22(7):1470–1481.Gai S, Yang P, Li C, Wang W, Dai Y, Niu N, Lin J. Adv Funct Mater. 2010; 20(7):1166.

11. Liu Z, Chen K, Davis C, Sherlock S, Cao QZ, Chen XY, Dai HJ. Cancer Res. 2008; 68:6652. [PubMed: 18701489] Tang ACL, Hwang GL, Tsai SJ, Chang MY, Tang ZCW, Tsai MD, Luo CY, Hoffman AS, Hsieh PCH. Plos One. 2012; 7

12. Matsumura Y, Maeda H. Cancer Res. 1986; 46:6387. [PubMed: 2946403]

13. Dani VA, Magyar A, Szász T. A Forum Hyperthermie. 2008; 1:8.Urano M, DE. Chemopotentiation by Hyperthermia. The Netherlands: VSP Utrecht; 1994. Dudar TE, Jain RK. Cancer Res. 1984; 44:605. [PubMed: 6692365] Kawasaki S, AJ.; Shibuya, K., et al. Thermotherapy for Neoplasia, Inflammation, and Pain. Kosaka M, ST.; Schmidt, KL.; Simon, E., editors. Tokyo: Springer Verlag; 2001. p. 424Vaupel P, Kallinowski F, Okunieff P. Cancer Res. 1989; 49:6449. [PubMed: 2684393]

14. Storm FK. Radiol Clin N Am. 1989; 27:621. [PubMed: 2648463]

15. Haase C, Nowak U. Phys Rev B. 2012; 85Kim DH, Nikles DE, Johnson DT, Brazel CS. J Magn Magn Mater. 2008; 320:2390.

16. Mikhaylov G, Mikac U, Magaeva AA, Itin VI, Naiden EP, Psakhye I, Babes L, Reinheckel T, Peters C, Zeiser R, Bogyo M, Turk V, Psakhye SG, Turk B, Vasiljeva O. Nat Nanotechnol. 2011; 6:594. [PubMed: 21822252] Paquet C, de Haan HW, Leek DM, Lin HY, Xiang B, Tian GH, Kell A, Simard B. Acs Nano. 2011; 5:3104. [PubMed: 21428441]

17. Kresge CT, Leonowicz ME, Roth WJ, Vartuli JC, Beck JS. Nature. 1992; 359:710.Vallet-Regi M, Balas F, Arcos D. Angew Chem Int Edit. 2007; 46:7548.Vallet-Regi M, Ramila A. Chem Mater. 2000; 12:961.

18. Lu J, Choi E, Tamanoi F, Zink JI. Small. 2008; 4:421. [PubMed: 18383576] Meng HA, Liong M, Xia TA, Li ZX, Ji ZX, Zink JI, Nel AE. Acs Nano. 2010; 4:4539. [PubMed: 20731437] Thomas CR, Ferris DP, Lee JH, Choi E, Cho MH, Kim ES, Stoddart JF, Shin JS, Cheon J, Zink JI. J Am Chem Soc. 2010; 132:10623. [PubMed: 20681678]

19. Harsh DC, Gehrke SH. J Control Release. 1991; 17:175.Kabra BG, Gehrke SH, Spontak RJ. Macromolecules. 1998; 31:2166.Zhu CL, Lu CH, Song XY, Yang HH, Wang XR. J Am Chem Soc. 2011; 133:1278. [PubMed: 21214180]

20. Reddy KS, Prabhakar MN, Reddy VN, Sathyamaiah G, Maruthi Y, Subha MCS, Rao KC. J Appl Polym Sci. 2012; 125:2289.

21. Kratz K, Hellweg T, Eimer W. Polymer. 2001; 42:6631.Liu QF, Zhang P, Qing AX, Lan YX, Lu MG. Polymer. 2006; 47:2330.

22. Hong JS, Stavis SM, Lacerda SHD, Locascio LE, Raghavan SR, Gaitan M. Langmuir. 2010; 26:11581. [PubMed: 20429539] Kazakov S, Levon K. Curr Pharm Design. 2006; 12:4713.

23. Kaida S, Cabral H, Kumagai M, Kishimura A, Terada Y, Sekino M, Aoki I, Nishiyama N, Tani T, Kataoka K. Cancer Res. 2010; 70:7031. [PubMed: 20685894] Nasongkla N, Bey E, Ren JM, Ai H,

Khemtong C, Guthi JS, Chin SF, Sherry AD, Boothman DA, Gao JM. Nano Lett. 2006; 6:2427. [PubMed: 17090068]

24. Seo WS, Lee JH, Sun XM, Suzuki Y, Mann D, Liu Z, Terashima M, Yang PC, McConnell MV, Nishimura DG, Dai HJ. Nat Mater. 2006; 5:971. [PubMed: 17115025]

25. Atkinson WJ, Brezovich IA, Chakraborty DP. Ieee T Bio-Med Eng. 1984; 31:70.

26. Adachi S, Kokura S, Okayama T, Ishikawa T, Takagi T, Handa O, Naito Y, Yoshikawa T. Int J Hyperther. 2009; 25:210.Baronzio GF, GA.; Baronzio, A., et al. Landes Bioscience. Austin, TX: 2000. Mosser DD, Caron AW, Bourget L, DenisLarose C, Massie B. Mol Cell Biol. 1997; 17:5317. [PubMed: 9271409] Ohnishi, KOaT. Annals of Cancer Research and Therapy. 2007; 15:6.

27. Ge JP, Hu YX, Biasini M, Beyermann WP, Yin YD. Angew Chem Int Edit. 2007; 46:4342.

28. Zhang Q, Ge JP, Goebl J, Hu YX, Lu ZD, Yin YD. Nano Res. 2009; 2:583.

29. Zhang Q, Ge JP, Goebl J, Hu YX, Sun YG, Yin YD. Adv Mater. 2010; 22:1905. [PubMed: 20526992]

30. Park KS, Tae J, Choi B, Kim YS, Moon C, Kim SH, Lee HS, Kim J, Kim J, Park J, Lee JH, Lee JE, Joh JW, Kim S. Nanomed-Nanotechnol. 2010; 6:263.
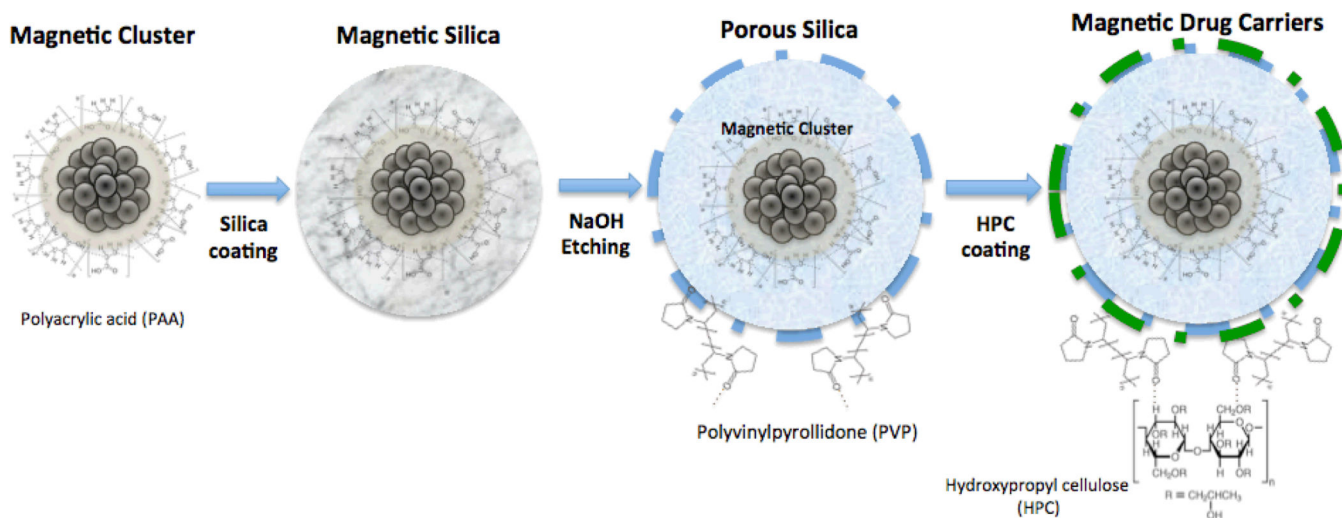
Figure 1.
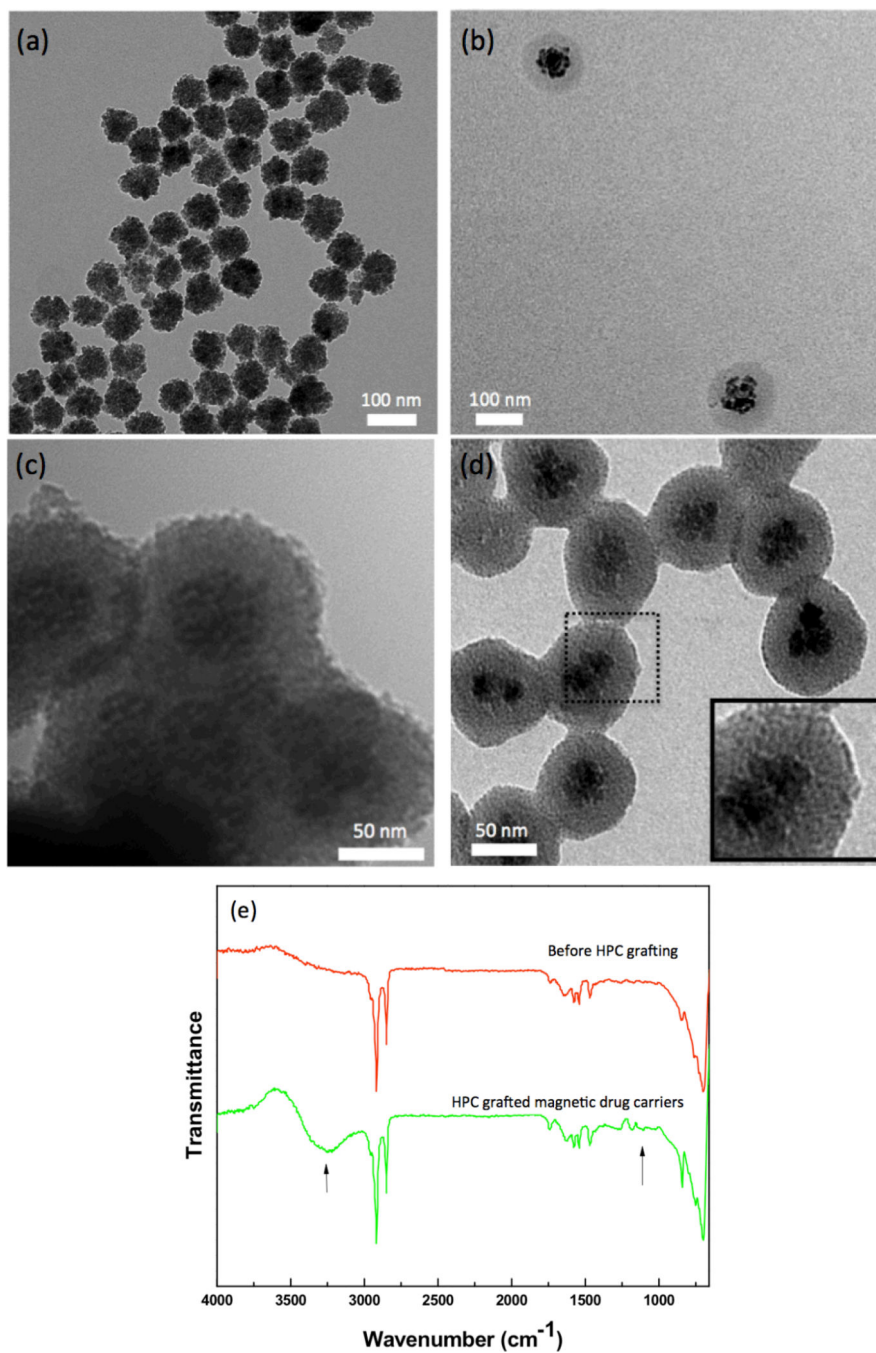Schematic describing chemical reactions for synthesis of magnetic drug carriers.

Figure 2.
TEM images of (a) USPIO clusters, (b) silica-coated USPIO clusters, (c) porous silica-shell USPIO clusters and (d) HPC grafted, porous silica-shell USPIO clusters (serving as magnetic drug carriers), (e) FT-IR spectra of magnetic drug carriers and HPC grafted magnetic drug carriers.
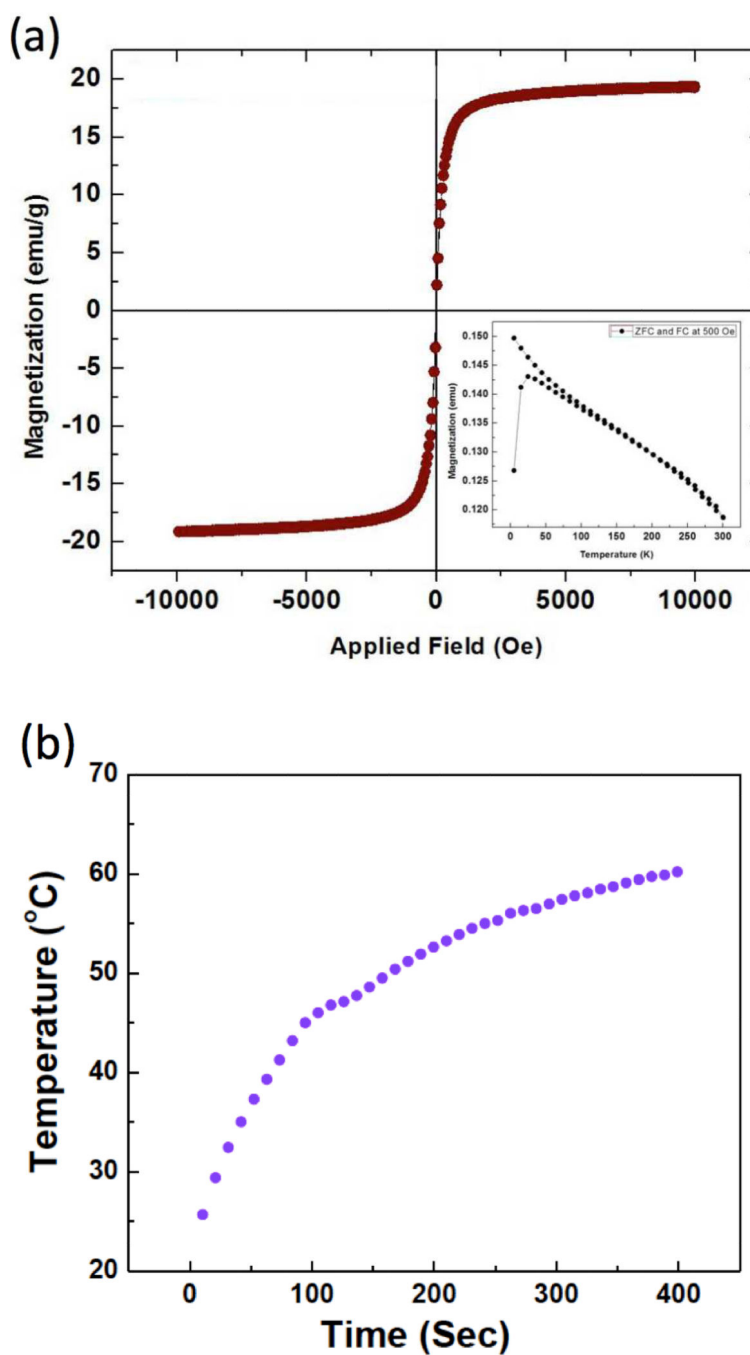
Figure 3.
(a) Magnetic characterization of magnetic drug carriers. Hysteresis loop and (inset) zero-field cooled/field cooled magnetization versus temperature measured with a 500 Oe field. (b) Heating profile of magnetic drug carriers (1ml;1 mg/ml) using a 175 Oe, 199kHz AC magnetic field.
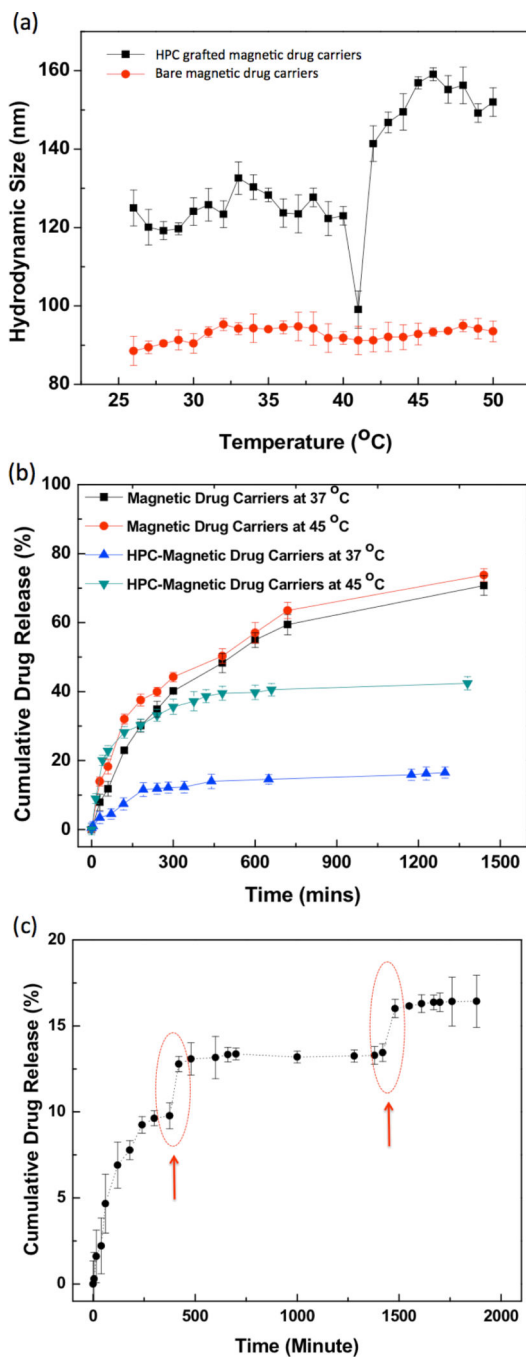
Figure 4.
(a) Temperature dependent hydrodynamic sizes of non-HPC grafted magnetic drug carriers and HPC grafted magnetic drug carriers in water. The concentration of these samples was 1 mg/ml, respectively, (b) Release of gemcitabine (GEM) from the magnetic drug carriers and HPC grafted magnetic drug carriers at 37 and 45 °C, (c) Heat triggered GEM release from these magnetic drug carriers. Red circles represent the 20 min heating periods (45 °C) during which the samples were irradiated with AC magnetic field (199 kHz, 175 Oe).
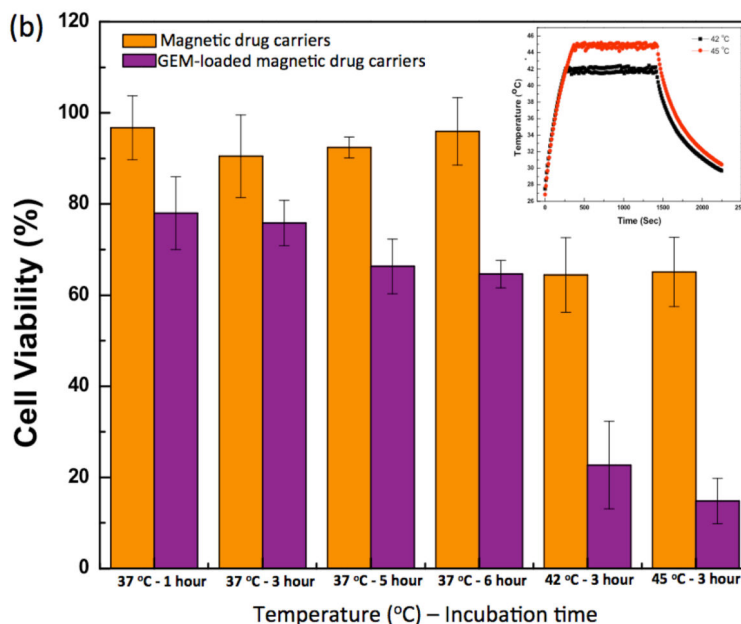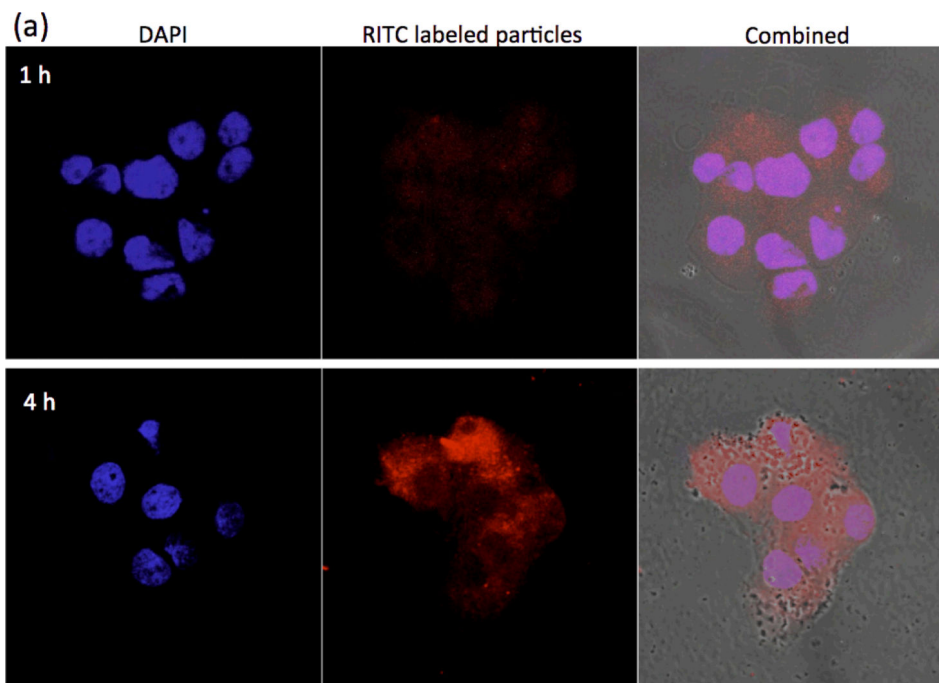
Figure 5.
(a) Confocal laser scanning microscopy images of PANC-1 cells after incubation with RITC labeled magnetic drug carriers (red fluorescence depicts magnetic drug carriers, DAPI blue fluorescence depicts the PANC-1 cell nuclei). Examples shown for both 1 h (top) and 4 h (bottom) incubation periods, (b) *In vitro* PANC-1 cell viability after exposure to either unloaded magnetic drug carriers and magnetic hyperthermia or concurrent GEM. chemohyperthermia using GEM-magnetic drug carriers and hyperthermia (concentration: 1 mg/ml).
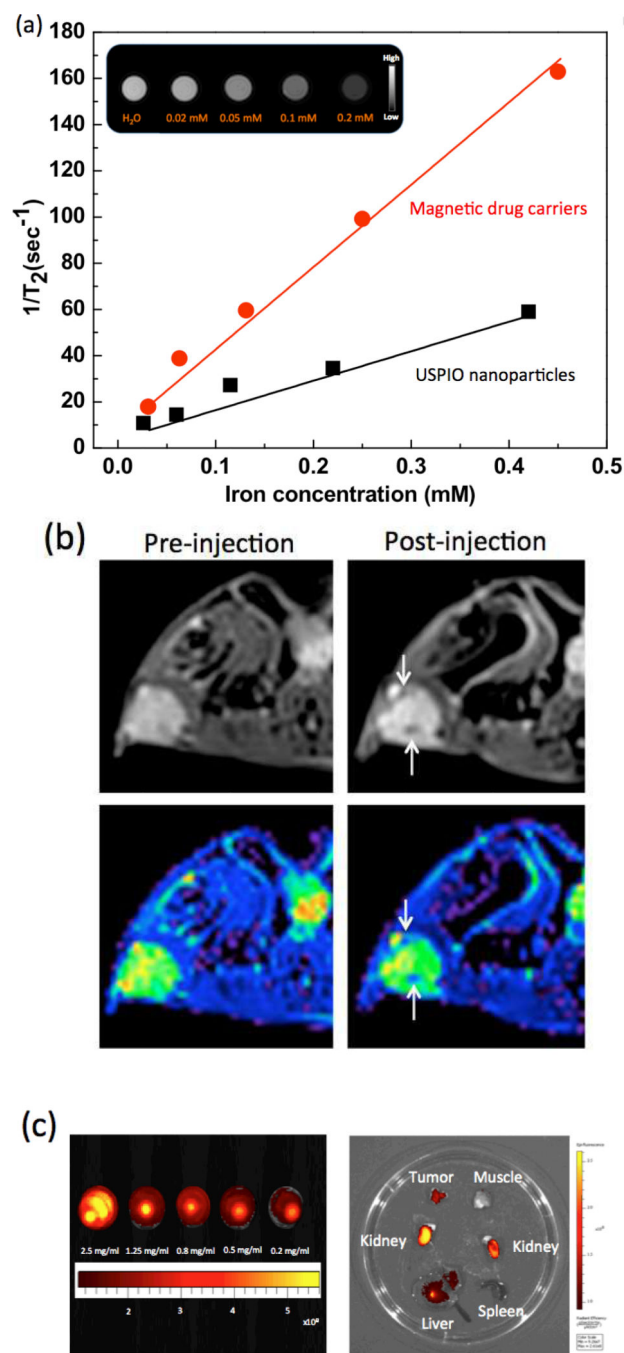
Figure 6.
Multimodal imaging of GEM-magnetic drug carriers. (a) Plots depicting the transverse relaxation rates ($1/T_2$, s^{-1}) measured at 7T in agar phantoms that included increasing concentrations (mM (Fe)) of magnetic drug carriers and USPIO nanoparticles. (inset) T_2-weighted MR images of agarose phantom at various concentrations of GEM-magnetic drug carriers, (b) (upper) *in vivo* T_2-weighted axial cross-section MR images and (lower) color maps of pre-injection and post-intravenous injection (arrows: signal reductions due to deposition of the magnetic drug carriers), and (c) (left) fluorescence image of cyto780 labeled GEM-magnetic drug carriers as a function of concentration ($\lambda_{ex}/\lambda_{em}$=783/800nm) and (right) *Ex vivo* fluorescence image of tumor tissue, muscle around tumor, kidney, spleen and liver after intravenous injection.

Figure 7.
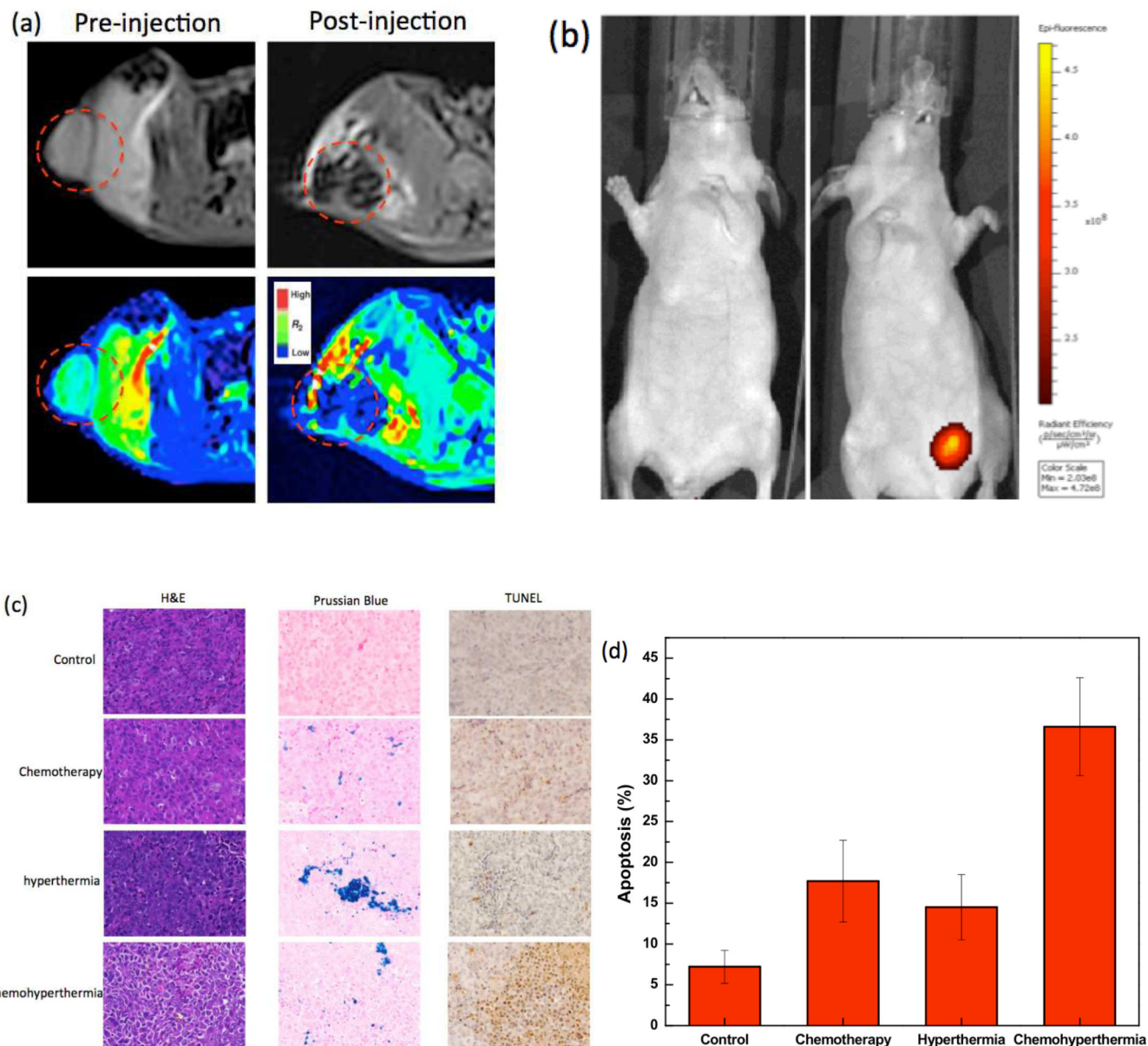
In vivo multimodal imaging of intratumoral injected GEM-magnetic drug carriers. (a) (upper) *in vivo* T_2-weighted axial cross section MR images and (lower) color maps of pre-injection and post-injection, (b) *in vivo* fluorescence image of (left) control and (right) cyto780 labeled GEM-magnetic drug carriers injected mouse ($\lambda_{ex}/\lambda_{em}$=783/800nm), (c) H&E, Prussian blue and TUNEL (terminal deoxynucleotidyl transferase mediated dUTP nick end-labeling) in tumor harvested from tumor bearing mice after treatments of GEM chemotherapy, hyperthermia and GEM chemohyperthermia, (d) Incidence of apoptosis in PANC-1 pancreatic tumor xenografts after the each treatment *in vivo*. Apoptotic index was determined by counting the percentage of apoptotic cells out of total tumor cells from five fields in each section. *p < 0.05, mean; bars, SD.